Overall viscoelastic properties of 2D and two-phase periodic composites constituted of elliptical and rectangular heterogeneities

Quy-Dong To, Sy Tuan Nguyen, Guy Bonnet, Minh Ngoc Vu

Overall viscoelastic properties of 2D and two-phase periodic composites constituted of elliptical and rectangular heterogeneities

Quy-Dong To [a, b, *], Sy-Tuan Nguyen [a, c], Guy Bonnet [b], Minh-Ngoc Vu [a]

[a] Duy Tan University, Institute of Research and Development, K7/25 Quang Trung, Da Nang, Vietnam
[b] Université Paris-Est, Laboratoire Modélisation et Simulation Multi Echelle, MSME UMR 8208 CNRS, 5 Boulevard Descartes, 77454 Marne-la-Vallée Cedex 2, France
[c] Euro-Engineering, Rue Jules Ferry, 64053 Pau, France

A B S T R A C T

This paper presents analytical solutions for the effective rheological viscoelastic properties of 2D periodic structures. The solutions, based on Fourier series analysis, are derived first in the Laplace-Carson (LC) space for different inclusion shapes (rectangle or ellipse) and arrangements. The effective results are obtained in the form of rational functions of the LC transform variable. Two inversion methods are used to find the relaxation behavior. The first one is based on the exact inverse of the LC transform while the second approximates the overall behavior by using a Standard Linear Solid model, which yields very simple analytical formulas for the coefficients entering the constitutive equations. Results of the two methods are compared in the case of an application to real materials.

Keywords:
Anisotropic viscoelasticity
Homogenization
Laplace-carson transform
2D periodic structure
Fourier analysis

1. Introduction

Viscoelasticity is a class of mechanical models that can describe effectively the time dependent behaviors of many materials like cement, concrete, polymer, glass or biomaterials, to name a few. At constant loading, those materials are deformed with time (creep) and vice versa, at constant strain, the internal stress changes with time (relaxation). These phenomena are more pronounced under high temperature conditions. Moreover, most materials are heterogeneous in nature, i.e. they are mixtures of ingredients of different characteristics, shapes and sizes. Materials that are both heterogeneous and viscoelastic are numerous, for example masonry walls composed of mortar and bricks, concrete made of granular and cement, polymer composites, etc..

From the structural engineering viewpoint, it is generally preferred to know the effective viscoelastic properties of the materials without being concerned by what happens inside. As a result, determining the overall behavior from the distribution of the ingredients becomes a distinct subject of interest. The usual approach consists in constructing a representative elementary volume (REV), solving the boundary value problem and finding the relation between the average stress and strain. This micromechanical method has proved to be powerful in estimating the effective elastic properties of the heterogeneous materials. From the study of different inclusion-matrix problems, analytical estimation schemes have been established including Mori-Tanaka, self-consistent, generalized self-consistent schemes, etc. (Eshelby, 1957; Mori and Tanaka, 1973; Christensen and Lo, 1979; Benveniste and Milton, 2003). Numerical methods are also developed to provide alternative solutions whenever analytical approach is impossible (Michel et al., 1999; Eyre and Milton, 1999; Monchiet and Bonnet, 2012). Bounds for the effective properties are also derived from the variational principle (Hashin and Shtrikman, 1963).

Although most of these important results are obtained for elastic materials, they can be translated to linear non ageing viscoelastic materials using the correspondence principle (Hashin, 1965, 1970; Christensen, 1969; Schapery, 1967; Wang and Weng, 1992; Kachanov, 1992; Lahellec and Suquet, 2007; Dormieux et al., 2006). It can be shown that in the Laplace-Carson (LC) transform space, the writing of the constitutive behavior is the same as in elasticity, the stiffness tensors being nevertheless functions of the LC transform variable (denoted thereafter LC variable). However, assuming that the solution in LC space is obtained, there are still considerable difficulties in obtaining the inverse LC

* Corresponding author. Duy Tan University, Institute of Research and Development, K7/25 Quang Trung, Da Nang, Vietnam.
E-mail addresses: quy-dong.to@u-pem.fr (Q.-D. To), stuan.nguyen@gmail.com (S.-T. Nguyen), guy.bonnet@u-pem.fr (G. Bonnet), vungocminh@dtu.edu.vn (M.-N. Vu).

transform to find the corresponding results in time space (Lévesque et al., 2007; Le et al., 2007).

The paper is concerned mainly by the viscoelastic behavior of 2D media which are frequently encountered in masonry structures, these structures being constituted of 2D walls. The system is composed of elastic inclusions distributed periodically in a viscoelastic matrix. The inclusions can have rectangular or elliptical shapes and they are located at sites of different 2D Bravais lattices. In LC space, we adopt the method of estimating the effective behavior based on spatial Fourier transform (Nemat-Nasser et al., 1982; To et al., 2016a; Hoang and Bonnet, 2013). Explicit and simple analytical results are found in many situations. Next, the inverse LC transform will be treated. Two methods are used and compared in this case. Based on the fact that the effective properties are rational functions of LC variable, the first method computes exactly the inverse transform and finds the relaxation function. The second method proceeds in approximating the overall behavior by using a rheological Standard Linear Solids (SLS) model (identical to the one of the matrix phase) and in finding the physical parameters by studying long term and short term behaviors. We emphasize here that the effective SLS model is generally not exactly equivalent to the exact overall viscoelastic behavior of the material. A shown by Suquet (2012), the effective behavior of a mixture of viscoelastic materials having the Maxwell behavior will not have the same kind of behavior (i.e. here of Maxwell type). However by determining relevant model parameters, we can obtain an approximate effective SLS model having several features similar to the equivalent homogeneous material. Numerical experiences on different composite materials have shown very often that the behavior of mixtures of SLS matrix and elastic inclusions (including voids or cracks) can be modeled by using the same kind of behavior as the matrix with good accuracy. Different tests done in the present paper also show that the full effective model and the approximate effective model are very close. The following sections will be dedicated to the detailed development of those ideas.

2. Viscoelastic behavior of 2 phase periodic composite in Laplace-Carson space

2.1. Homogenization of periodic heterogeneous viscoelastic materials

Before proceeding, let us introduce first the notations for Fourier transform and Laplace-Carson (LC) transform used in this paper. Since our problem involves 2D periodic functions, it is relevant to use the Fourier series analysis. Generally, any spatially periodic function $\varphi(\boldsymbol{x},t)$, i.e. periodic with respect to $\boldsymbol{x}$, can be expressed as a Fourier series

$$\varphi(\boldsymbol{x},t)=\sum_{\xi}\varphi(\xi,t)e^{i\xi.\boldsymbol{x}},\quad \varphi(\xi,t)=\frac{1}{V}\int_{V}\varphi(\boldsymbol{x},t)e^{-i\xi.\boldsymbol{x}}d\boldsymbol{x} \tag{1}$$

where $\varphi(\xi,t)$ denotes the spatial Fourier transform of $\varphi(\boldsymbol{x},t)$, V the rectangular unit cell of dimensions $a_1\times a_2$ and ξ the wave vectors whose components ξ_1,ξ_2 are given as follows

$$\xi_i=\frac{2\pi n_i}{a_i},\quad i=1,2,\quad n_i\in\mathbb{Z} \tag{2}$$

where the Einstein's summation convention for repeated index is not considered. On the other hand, problems involving viscoelastic behavior can be solved by using the correspondence principle and LC transform. As a notation, we use φ^* (star * as superscript) for the LC transform of the time dependent function φ, for example

$$\varphi^*(\boldsymbol{x},s)=s\int_0^{\infty}\varphi(\boldsymbol{x},t)e^{-st}dt \tag{3}$$

In this paper, we are interested in the overall properties of two phase viscoelastic composites. The materials under consideration contain heterogeneities of arbitrary shapes ω periodically embedded in a matrix material (Fig. 2). In LC space, the local constitutive behavior can be written as follows

$$\boldsymbol{\sigma}^*(\boldsymbol{x},s)=\mathbb{C}^*(\boldsymbol{x},s):\boldsymbol{\varepsilon}^*(\boldsymbol{x},s) \tag{4}$$

where $\mathbb{C}^*(\boldsymbol{x},s)=\mathbb{C}_0^*(s)$ for matrix ($\boldsymbol{x}\notin\omega$) and $\mathbb{C}^*(\boldsymbol{x},s)=\mathbb{C}_1^*(s)$ for inclusions ($\boldsymbol{x}\in\omega$). To find the effective behavior of the material $\mathbb{C}^{e*}(s)$, we need to solve the localization problem in a representative elementary volume (REV) and find the linear relation between average stress $\boldsymbol{\Sigma}^*(s)$ and strain $\mathbf{E}^*(s)$, namely

$$\begin{aligned}&\boldsymbol{\Sigma}^*(s)=\mathbb{C}^{e*}(s):\mathbf{E}^*(s),\quad \boldsymbol{\Sigma}^*(s)=\frac{1}{V}\int_V\boldsymbol{\sigma}^*(\boldsymbol{x},s)d\boldsymbol{x},\\ &\mathbf{E}^*(s)=\frac{1}{V}\int_V\boldsymbol{\varepsilon}^*(\boldsymbol{x},s)d\boldsymbol{x}\end{aligned} \tag{5}$$

In principle, the size of a REV must be large enough to contain all the information on the distribution of heterogeneities within the material. However, for periodic media, it is sufficient to solve a localization problem in the unit cell V under the periodicity conditions of the local stress field $\boldsymbol{\sigma}^*(\boldsymbol{x},s)$ and strain field $\boldsymbol{\varepsilon}^*(\boldsymbol{x},s)$.

The theory presented in this paper can be applied to any viscoelastic material. Nevertheless, we shall only deal with special cases where the heterogeneities are linearly elastic and the matrix is viscoelastic corresponding to a Standard Linear Solid (LSL). The behavior of the latter is modeled by a rheological model made up of three elements (two springs and one dash-pot) as shown in Fig. 1. It is a Maxwell series in parallel with the second spring that defines the long term elastic behavior of the material. In LC space, the elastic stiffness of the equivalent elastic material is a function of the LC variable s and of the properties of the rheological elements (see also Nguyen et al., 2011). In this case, this dependency is expressed as:

$$\mathbb{C}_0^*(s)=\left(\mathbb{C}_M^{-1}+\frac{1}{s}\mathbb{C}_v^{-1}\right)^{-1}+\mathbb{C}_\infty \tag{6}$$

where $\mathbb{C}_M$ is the elastic stiffness tensor corresponding to the spring of the Maxwell series, $\mathbb{C}_v$ the viscosity tensor of the dash-pot and $\mathbb{C}_\infty$ the elastic stiffness tensor of the second spring that corresponds also to the long-term elastic behavior of the material.

Assuming that the matrix is isotropic, we can write the viscoelastic tensors in (6)

$$\begin{aligned}\mathbb{C}_M&=3k_M\mathbb{J}+2\mu_M\mathbb{K},\quad \mathbb{C}_v=3k_v\mathbb{J}+2\mu_v\mathbb{K},\quad \mathbb{C}_\infty\\ &=3k_\infty\mathbb{J}+2\mu_\infty\mathbb{K}\end{aligned} \tag{7}$$

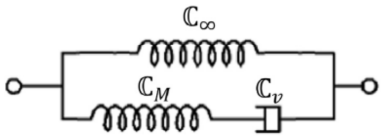

Fig. 1. The Standard Linear Solid model used for the matrix and the effective material.

using the bulk and shear constants $k_M, \mu_M, k_\nu, \mu_\nu, k_\infty, \mu_\infty$. The fourth order projection tensors $\mathbb{J}$ and $\mathbb{K}$ are defined from the fourth order identity tensor $\mathbb{I}$ and the second order identity tensor $\boldsymbol{I}$ via the relation

$$\mathbb{J} = \frac{1}{3}\boldsymbol{I}\otimes\boldsymbol{I}, \quad \mathbb{K} = \mathbb{I} - \mathbb{J} \tag{8}$$

Finally, we can now express $\mathbb{C}_0^*(s)$ via the constants $k_M, \mu_M, k_\nu, \mu_\nu, k_\infty, \mu_\infty$ as follows

$$\mathbb{C}_0^*(s) = 3k_0^*(s)\mathbb{J} + 2\mu_0^*(s)\mathbb{K},$$
$$k_0^*(s) = \left(\frac{1}{k_M} + \frac{1}{sk_\nu}\right)^{-1} + k_\infty, \quad \mu_0^*(s) = \left(\frac{1}{\mu_M} + \frac{1}{s\mu_\nu}\right)^{-1} + \mu_\infty \tag{9}$$

The heterogeneities are also isotropic and their stiffness tensor can be written in terms of constants k_1, μ_1 as

$$\mathbb{C}_1^* = \mathbb{C}_1 = 3k_1\mathbb{J} + 2\mu_1\mathbb{K} \tag{10}$$

2.2. Periodic Eshelby and Hill tensors and estimation of overall properties

In this section, we summarize briefly some results on the homogenization of periodic materials issued from the work of Nemat-Nasser et al. (1982) and applied to 2D structures. Here, the two Eshelby problems are presented in the periodic setting and the links between the Eshelby tensor, Hill tensor (Hill, 1965) and the overall properties are established for an arbitrary inclusion shape. All the following expressions are written in the LC space (star * as superscript) and LC variable s is dropped for the sake of clarity.

The first Eshelby problem involves a homogeneous elastic material of stiffness $\mathbb{C}_0^*$ subject to a prescribed V-periodic eigenstrain field $\tilde{\boldsymbol{\varepsilon}}^*$ and zero macroscopic strain. The induced strain field is also periodic and can be computed by the formula

$$\boldsymbol{\varepsilon}^* = \boldsymbol{\Gamma}^{0*}(\mathbb{C}_0^* : \tilde{\boldsymbol{\varepsilon}}^*) \tag{11}$$

where Γ^{0*}_{ijkl} is the Green operator. In the Fourier space, the 2D Green operator $\Gamma^{0*}_{ijkl}(\boldsymbol{\xi})$ admits the analytical expression

$$\begin{aligned}\Gamma^{0*}_{ijkl}(\boldsymbol{\xi}) &= \frac{1}{4\mu_0^*}\left(\delta_{ik}\bar{\xi}_j\bar{\xi}_l + \delta_{il}\bar{\xi}_j\bar{\xi}_k + \delta_{jk}\bar{\xi}_i\bar{\xi}_l + \delta_{jl}\bar{\xi}_i\bar{\xi}_k\right) \\ &\quad - \frac{k_0^* + \frac{1}{3}\mu_0^*}{\mu_0^*\left(k_0^* + \frac{4}{3}\mu_0^*\right)}\bar{\xi}_i\bar{\xi}_j\bar{\xi}_k\bar{\xi}_l, \quad \bar{\xi}_i \\ &= \frac{\xi_i}{\xi} \text{ with } i = 1,2 \text{ and } \xi = \sqrt{\xi_1^2 + \xi_2^2}\end{aligned} \tag{12}$$

In the special case where $\tilde{\boldsymbol{\varepsilon}}^*$ is constant inside a geometrical region w in V and vanishes outside, for example

$$\tilde{\boldsymbol{\varepsilon}}^* = \chi^\omega(\boldsymbol{x})\tilde{\boldsymbol{E}}^*, \quad \chi^\omega(\boldsymbol{x}) = 1 \text{ if } \boldsymbol{x}\in\omega, \quad \chi^\omega(\boldsymbol{x}) = 0 \text{ if } \boldsymbol{x}\notin\omega \tag{13}$$

the strain field is then linear in $\tilde{\boldsymbol{E}}^*$ via the periodic Eshelby tensor field $\mathbb{S}^*$. The latter meets the following relations:

$$\boldsymbol{\varepsilon}^*(\boldsymbol{x}) = \mathbb{S}^*(\boldsymbol{x}) : \tilde{\boldsymbol{E}}^*, \quad \mathbb{S}^*(\boldsymbol{x}) = \boldsymbol{\Gamma}^{0*}(\mathbb{C}_0^*\chi) \tag{14}$$

Generally, the strain field and the periodic Eshelby tensor field are not uniform in ω, except for ellipsoidal shapes embedded in a very large volume V. However, we can average those quantities over the inclusion volume ω and obtain the relation

$$\langle\boldsymbol{\varepsilon}^*\rangle_\omega = \langle\mathbb{S}^*\rangle_\omega : \tilde{\boldsymbol{E}}^* \tag{15}$$

in which $\langle\mathbb{S}^*\rangle_\omega$ can be computed explicitly as follows

$$\langle\mathbb{S}^*\rangle_\omega = \sum_{\boldsymbol{\xi}\neq 0} g(\boldsymbol{\xi})\boldsymbol{\Gamma}^{0*}(\boldsymbol{\xi})\mathbb{C}_0^*, \quad g(\boldsymbol{\xi}) = f^{-1}\chi^\omega(\boldsymbol{\xi})\chi^\omega(-\boldsymbol{\xi}) \tag{16}$$

The quantity f denotes the inclusion fraction and $\chi^\omega(\boldsymbol{\xi})$ the form factor of the latter which is defined as the Fourier transform of the indicator function $\chi^\omega(\boldsymbol{x})$. It is also interesting to define the periodic Hill tensor as $\mathbb{P}^* : \mathbb{C}_0^* = \mathbb{S}^*(\boldsymbol{x})$ whose average is equal to

$$\langle\mathbb{P}^*\rangle_\omega = \sum_{\boldsymbol{\xi}\neq 0} g(\boldsymbol{\xi})\boldsymbol{\Gamma}^{0*}(\boldsymbol{\xi}), \tag{17}$$

In the second Eshelby problem, the region w is replaced by a material of different stiffness $\mathbb{C}_1^*$ and the new composite material is subject to a macroscopic strain $\boldsymbol{E}^*$. The problem can be reformulated by considering that the material is homogeneous again with elasticity tensor $\mathbb{C}_0^*$, like in the first Eshelby problem. However, the equivalent eigenstrain field $\tilde{\boldsymbol{\varepsilon}}^*$ in the new problem is defined as

$$(\mathbb{C}_0^* - \mathbb{C}_1^*) : \boldsymbol{\varepsilon}^* = \mathbb{C}_0^* : \tilde{\boldsymbol{\varepsilon}}^* \quad \text{if } \boldsymbol{x}\in\omega, \quad \tilde{\boldsymbol{\varepsilon}}^* = 0 \text{ if } \boldsymbol{x}\notin\omega \tag{18}$$

The strain field $\boldsymbol{\varepsilon}^*$ of the material can be determined by superposing the two effects due to macroscopic strain and eigenstrain. Expressing $\boldsymbol{\varepsilon}^*$ in terms of $\tilde{\boldsymbol{\varepsilon}}^*$ yields the integral equation for $\tilde{\boldsymbol{\varepsilon}}^*$

$$\mathbb{C}_0^* : \tilde{\boldsymbol{\varepsilon}}^* = (\mathbb{C}_0^* - \mathbb{C}_1^*) : \left(\boldsymbol{E}^* + \boldsymbol{\Gamma}^{0*}(\mathbb{C}_0^* : \tilde{\boldsymbol{\varepsilon}}^*)\right), \quad \boldsymbol{x}\in\omega \tag{19}$$

Nemat-Nasser et al. (1982) proposed to estimate $\langle\tilde{\boldsymbol{\varepsilon}}^*\rangle_\omega$ based on (19). By averaging both sides over w and replacing the eigenstrain field $\tilde{\boldsymbol{\varepsilon}}^*$ in the convolution $\boldsymbol{\Gamma}^{0*}(\mathbb{C}_0^* : \tilde{\boldsymbol{\varepsilon}}^*)$ by its average $\langle\tilde{\boldsymbol{\varepsilon}}^*\rangle_\omega$, they derived the equation

$$\mathbb{C}_0^* : \langle\tilde{\boldsymbol{\varepsilon}}^*\rangle_\omega = (\mathbb{C}_0^* - \mathbb{C}_1^*) : (\boldsymbol{E}^* + \langle\mathbb{S}^*\rangle_\omega : \langle\tilde{\boldsymbol{\varepsilon}}^*\rangle_\omega) \tag{20}$$

After obtaining $\langle\tilde{\boldsymbol{\varepsilon}}^*\rangle_\omega$ from (20), the effective stiffness $\mathbb{C}^{e*}$ can be determined with the formula

$$\mathbb{C}^{e*} = \mathbb{C}_0^* + f\left[(\mathbb{C}_1^* - \mathbb{C}_0^*)^{-1} + \langle\mathbb{P}^*\rangle_\omega\right]^{-1} \tag{21}$$

2.3. Results for plane strain problems

From (12) and (17), we can recast the average Hill tensor in the following form

$$\langle\mathbb{P}^*\rangle_\omega = \frac{1}{2\mu_0^*}\mathbb{W} - \frac{k_0^* + \frac{1}{3}\mu_0^*}{\mu_0^*\left(k_0^* + \frac{4}{3}\mu_0^*\right)}\mathbb{U} \tag{22}$$

where $\mathbb{W}$ and $\mathbb{U}$ are the fourth order tensors that are only functions of the geometry and distribution of the inclusions given by:

$$\mathbb{W} = \begin{bmatrix} 2S_1 & 0 & 0 \\ 0 & 2S_2 & 0 \\ 0 & 0 & S_1 + S_2 \end{bmatrix}, \quad \mathbb{U} = \begin{bmatrix} S_3 & S_5 & 0 \\ S_5 & S_4 & 0 \\ 0 & 0 & 2S_5 \end{bmatrix} \tag{23}$$

in Kelvin's matrix notation. The scalars S_1 to S_5 are the lattice sums given by:

$$S_i = \sum_{\xi\neq 0} g(\boldsymbol{\xi})\bar{\xi}_i^2, \quad S_{i+2} = \sum_{\xi\neq 0} g(\boldsymbol{\xi})\bar{\xi}_i^4, \quad S_5 = \sum_{\xi\neq 0} g(\boldsymbol{\xi})\bar{\xi}_1^2\bar{\xi}_2^2, \quad i = 1,2 \tag{24}$$

and verifying the properties

$$S_1 + S_2 = S_3 + S_4 + 2S_5 = 1 - f, \quad S_3 + S_5 = S_1, \quad S_4 + S_5 = S_2 \tag{25}$$

It is now possible to obtain all the elements of $\mathbb{C}^{e*}$ based on (21). Of all the components, the expression for the shear stiffness C_{1212}^{e*} is the simplest, for example

$$C_{1212}^{e*} = \mu_0^* + \frac{f\mu_0^*}{\frac{\mu_0^*}{\delta\mu^*} + (1-f) - 4\frac{k_0^*+\mu_0^*/3}{k_0^*+4\mu_0^*/3}S_5} \tag{26}$$

To derive (26), we have made use of the property $S_1 + S_2 = 1 - f$. Denoting $\delta\mu^* = \mu_1^* - \mu_0^*$ and $\delta k^* = k_1^* - k_0^*$, we can compute explicitly all the remaining components. The final results are more cumbersome than C_{1212}^{e*} and they are listed as follows

$$C_{1111}^{e*} = k_0^* + \frac{4}{3}\mu_0^* + \frac{f}{\Delta}\left[\frac{S_2}{\mu_0^*} - \frac{\left(k_0^* + \frac{1}{3}\mu_0^*\right)S_4}{\mu_0^*\left(k_0^* + \frac{4}{3}\mu_0^*\right)} + \frac{\left(\delta k^* + \frac{4}{3}\delta\mu^*\right)}{4\delta\mu^*\left(\delta k^* + \frac{1}{3}\delta\mu^*\right)}\right],$$

$$C_{2222}^{e*} = k_0^* + \frac{4}{3}\mu_0^* + \frac{f}{\Delta}\left[\frac{S_1}{\mu_0^*} - \frac{\left(k_0^* + \frac{1}{3}\mu_0^*\right)S_3}{\mu_0^*\left(k_0^* + \frac{4}{3}\mu_0^*\right)} + \frac{\left(\delta k^* + \frac{4}{3}\delta\mu^*\right)}{4\delta\mu^*\left(\delta k^* + \frac{1}{3}\delta\mu^*\right)}\right],$$

$$C_{1122}^{e*} = k_0^* - \frac{2}{3}\mu_0^* + \frac{f}{\Delta}\left[\frac{\delta k^* - \frac{2}{3}\delta\mu^*}{4\delta\mu^*\left(\delta k^* + \frac{1}{3}\delta\mu^*\right)} + \frac{\left(k_0^* + \frac{1}{3}\mu_0^*\right)S_5}{\mu_0^*\left(k_0^* + \frac{4}{3}\mu_0^*\right)}\right],$$

$$\Delta = \left[\frac{S_1}{\mu_0^*} - \frac{\left(k_0^* + \frac{1}{3}\mu_0^*\right)S_3}{\mu_0^*\left(k_0^* + \frac{4}{3}\mu_0^*\right)} + \frac{\left(\delta k^* + \frac{4}{3}\delta\mu^*\right)}{4\delta\mu^*\left(\delta k^* + \frac{1}{3}\delta\mu^*\right)}\right]\left[\frac{S_2}{\mu_0^*} - \frac{\left(k_0^* + \frac{1}{3}\mu_0^*\right)S_4}{\mu_0^*\left(k_0^* + \frac{4}{3}\mu_0^*\right)} + \frac{\left(\delta k^* + \frac{4}{3}\delta\mu^*\right)}{4\delta\mu^*\left(\delta k^* + \frac{1}{3}\delta\mu^*\right)}\right] - \left[\frac{\delta k^* - \frac{2}{3}\delta\mu^*}{4\delta\mu^*\left(\delta k^* + \frac{1}{3}\delta\mu^*\right)} + \frac{\left(k_0^* + \frac{1}{3}\mu_0^*\right)S_5}{\mu_0^*\left(k_0^* + \frac{4}{3}\mu_0^*\right)}\right]^2 \tag{27}$$

For materials with square symmetry, for example containing squared or circular inclusions ω within a squared unit cell V, we have the properties

$$S_1 = S_2 = \frac{1-f}{2}, \quad S_3 = S_4, \quad C_{1111}^{e*} = C_{2222}^{e*} \tag{28}$$

which allows to compute the 2D bulk modulus

$$\kappa^{e*} = \frac{1}{2}\left(C_{1111}^{e*} + C_{1122}^{e*}\right) = \kappa_0^* + \frac{f}{\frac{1-f}{\kappa_0^*+\mu_0^*} + \frac{1}{\delta\kappa^*}}, \tag{29}$$

Remark that under plane strain condition, the bulk modulus for an isotropic material is defined as $\kappa = k + \mu/3$. For materials with square symmetry, it is the volume response to isotropic stress in the plane 1–2. In principle, if we want to approximate the anisotropic materials by an isotropic behavior, we can choose the bulk modulus in (29) and the shear modulus $\mu^{e*} = C_{1212}^{e*}$ in (26). In this case, the overall constitutive law in the plane 1–2 reads

$$\Sigma_{ij}^* = \kappa^{e*}E_{kk}^*\delta_{ij} + 2\mu^{e*}\left(E_{ij}^* - \frac{1}{2}E_{kk}^*\right), \quad i,j,k = 1,2 \tag{30}$$

2.4. Consideration of inclusion shape and arrangement

By definition, the form factor $\chi^{\omega}(\boldsymbol{\xi})$ is the Fourier transform of the characteristic function $\chi^{\omega}(\boldsymbol{x})$, viz

$$\chi^{\omega}(\boldsymbol{\xi}) = \frac{1}{V}\int_{\omega} e^{-i\boldsymbol{\xi}\cdot\boldsymbol{x}}d\boldsymbol{x} \tag{31}$$

Analytical solutions $\chi^{\omega}(\boldsymbol{\xi})$ exist for many single inclusion shapes, for example ellipse, rectangles or polygons (Nemat-Nasser and Hori, 1993). They can be centered or not at the origin, aligned or not with the system of axes. Note that for any affine transformation $\boldsymbol{x} = \boldsymbol{L}.\boldsymbol{x}' - \boldsymbol{x}_{\boldsymbol{c}}$ that transforms ω' into ω, we can always relate the form factor for ω and ω',

$$\frac{1}{V}\int_{\omega} e^{-i\boldsymbol{\xi}\cdot\boldsymbol{x}}d\boldsymbol{x} = \frac{|J|}{V}e^{i\boldsymbol{\xi}\cdot\boldsymbol{x}_{\boldsymbol{c}}}\int_{\omega} e^{-i\boldsymbol{\xi}'\cdot\boldsymbol{x}'}d\boldsymbol{x}', \quad \boldsymbol{\xi}' = \boldsymbol{L}^{\boldsymbol{T}}\boldsymbol{\xi}, \quad or\chi^{\omega}(\boldsymbol{\xi}) = \left|J\right|e^{i\boldsymbol{\xi}\cdot\boldsymbol{x}_{\boldsymbol{c}}}\chi^{\omega'}(\boldsymbol{\xi}') \tag{32}$$

where $|J| = \det(\boldsymbol{L})$ is the Jacobian of the transformation that is constant for the affine transformations. This relation allows us to compute the form factor of any inclusion that is obtained by translating, rotating or uniformly deforming a reference inclusion.

Next, those inclusions can be located on sites of different 2D

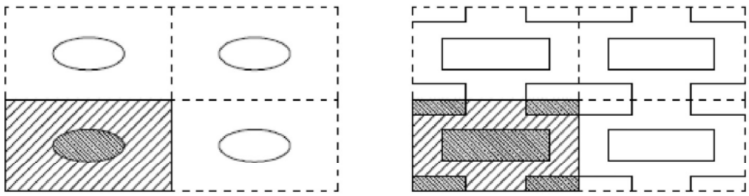

Fig. 2. Elliptical and rectangular inclusions arranged in PR (left) and CR lattices (right).

Bravais lattices. Explicit expressions for all type of lattices can be obtained. However, we shall only focus on rectangular and elliptical shapes whose principal axes are aligned with the system of axes 1,2. Two different arrangements are considered: centered rectangular lattice (CR) or primitive rectangular (PR) lattice (see Fig. 2).

The functions $g(\xi)$ according to (16) for different configurations are given below (Nemat-Nasser and Hori, 1993).

For elliptical inclusion of semi axes $b_1,\ b_2$

$$\begin{aligned}&\text{PR lattice}: \quad g(\boldsymbol{\xi}) = 4f\left[\frac{J_1(\eta)}{\eta}\right]^2,\\ &\text{CR lattice}: \quad g(\boldsymbol{\xi}) = f\left[\frac{J_1(\eta)}{\eta}\left(1+(-1)^{n_1+n_2}\right)\right]^2,\\ &\eta_i = \xi_i b_i, \quad \eta = \sqrt{\eta_1^2+\eta_2^2}\end{aligned} \tag{33}$$

where $J_1(\eta)$ is the Bessel function of first kind and first order.

For rectangular inclusion of dimensions $2b_1,\ 2b_2$

$$\begin{aligned}&\text{PR lattice}: \quad g(\boldsymbol{\xi}) = f[\text{sinc}(\eta_1)\text{sinc}(\eta_2)]^2,\\ &\text{CR lattice}: \quad g(\boldsymbol{\xi}) = \frac{f}{4}\left[\text{sinc}(\eta_1)\text{sinc}(\eta_2)\left(1+(-1)^{n_1+n_2}\right)\right]^2,\end{aligned} \tag{34}$$

where sinc denotes cardinal sin function.

2.5. Analytical estimation of lattice sums

As shown above, the quantities S_1 to S_5 are the lattice sums in the reciprocal space. To et al. (2013, 2016a) showed that it is possible to simplify the computation of those sums by keeping some leading terms, i.e. those near the origin and estimate the remainder by a continuous integral. This approach has proved to yield simple analytical solutions for spherical and ellipsoidal shapes with high accuracy. In this paper, we shall employ the same method to study 2D structures. For example, using the dimensionless wave vector $\boldsymbol{\eta}(\eta_1,\ \eta_2)$ and the aspect ratio $\alpha = \frac{b_2}{b_1}$, we can rewrite the lattice sum S_1 for elliptical shapes and PR lattice as

$$S_1 \approx 4f\sum_{\eta\le\eta_c}\left[\frac{J_1(\eta)}{\eta}\right]^2\frac{\alpha^2\eta_1^2}{\alpha^2\eta_1^2+\eta_2^2} + \frac{1}{\pi}\int_{\eta=\eta_c}^{\infty}\frac{\alpha^2\eta_1^2}{\alpha^2\eta_1^2+\eta_2^2}\left[\frac{J_1(\eta)}{\eta}\right]^2 d\boldsymbol{\eta} \tag{35}$$

The cutoff radius η_c is chosen to account for the finite sum of terms related to values of η near the origin. From a practical viewpoint, it is sufficient to choose $\eta_c = 4\varepsilon, \quad \varepsilon = \max\left(\frac{2\pi b_1}{a_1}, \frac{2\pi b_2}{a_2}\right)$. Regarding the integral on the right hand side (RHS) of (24), it can be computed explicitly without difficulties by introducing the orientation θ between the wave vector and the first coordinate axis:

$$\frac{1}{\pi}\int_{\eta=\eta_c}^{\infty}\frac{\alpha^2\eta_1^2}{\alpha^2\eta_1^2+\eta_2^2}\left[\frac{J_1(\eta)}{\eta}\right]^2 d\boldsymbol{\eta} = \frac{1}{\pi}\int_{\eta=\eta_c}^{\infty}\left[\frac{J_1(\eta)}{\eta}\right]^2\eta d\eta\int_0^{2\pi}\frac{\alpha^2\cos^2\theta d\theta}{\alpha^2\cos^2\theta+\sin^2\theta} \tag{36}$$

Let us define $\varphi(n_1,n_2)$ as function of lattice point (n_1,n_2), namely.

$$\begin{aligned}&\text{PR lattice}: \quad \varphi(n_1,n_2) = 1 \quad \forall n_1,n_2,\\ &\text{CR lattice}: \quad \varphi(n_1,n_2) = \left[1+(-1)^{n_1+n_2}\right]/2,\end{aligned} \tag{37}$$

For CR arrangement, $\varphi(n_1,n_2) = 1$ if n_1,n_2 are both odd or even, otherwise $\varphi(n_1,n_2) = 0$. The final results for $S_1,\ S_2,\ \ldots,S_5$ for both lattice types are listed in the following

$$S_1 \approx 4f\sum_{\eta\le\eta_c}\left[\frac{J_1(\eta)}{\eta}\varphi\right]^2\frac{\alpha^2\eta_1^2}{\alpha^2\eta_1^2+\eta_2^2} + \frac{\alpha}{(\alpha+1)}\left[J_0^2(\eta_c)+J_1^2(\eta_c)\right] \tag{38}$$

$$S_2 \approx 4f\sum_{\eta\le\eta_c}\left[\frac{J_1(\eta)}{\eta}\varphi\right]^2\frac{\eta_2^2}{\alpha^2\eta_1^2+\eta_2^2} + \frac{1}{(\alpha+1)}\left[J_0^2(\eta_c)+J_1^2(\eta_c)\right] \tag{39}$$

$$S_3 \approx 4f\sum_{\eta\le\eta_c}\left[\frac{J_1(\eta)}{\eta}\varphi\right]^2\left[\frac{\alpha^2\eta_1^2}{\alpha^2\eta_1^2+\eta_2^2}\right]^2 + \frac{\alpha(2\alpha+1)}{2(\alpha+1)^2}\left[J_0^2(\eta_c)+J_1^2(\eta_c)\right] \tag{40}$$

$$S_4 \approx 4f \sum_{\eta \le \eta_c} \left[\frac{J_1(\eta)}{\eta}\varphi\right]^2 \left[\frac{\eta_2^2}{\alpha^2\eta_1^2+\eta_2^2}\right]^2 + \frac{(\alpha+2)}{2(\alpha+1)^2}\left[J_0^2(\eta_c)+J_1^2(\eta_c)\right] \tag{41}$$

$$S_5 \approx 4f \sum_{\eta \le \eta_c} \left[\frac{J_1(\eta)}{\eta}\varphi\right]^2 \frac{\alpha^2\eta_1^2\eta_2^2}{(\alpha^2\eta_1^2+\eta_2^2)^2} + \frac{\alpha}{2(\alpha+1)^2}\left[J_0^2(\eta_c)+J_1^2(\eta_c)\right] \tag{42}$$

It is clear that when $\varepsilon \to 0$ (or $f \to 0$), we recover the results for an isolated ellipse in an infinite matrix

$$S_1 = \frac{\alpha}{(\alpha+1)}, \quad S_2 = \frac{1}{(\alpha+1)}, \quad S_3 = \frac{\alpha(2\alpha+1)}{2(\alpha+1)^2}, \quad S_4 = \frac{(\alpha+2)}{2(\alpha+1)^2}, \quad S_5 = \frac{\alpha}{2(\alpha+1)^2} \tag{43}$$

which are independent of lattice types and volume fraction. For circular inclusion, we obtain

$$S_1 = S_2 = \frac{1}{2}, \quad S_3 = S_4 = \frac{3}{8}, \quad S_5 = \frac{1}{8}, \tag{44}$$

Analytical approximations for rectangular inclusions can also be obtained in the same way. However, the results for the general cases are much more cumbersome, even when handled by symbolic calculation software like Maple or Mathematica. Results for the limit case $\varepsilon \to 0$ (or $f \to 0$, isolated rectangle in an infinite matrix) are simpler and more interesting

$$S_1 = \frac{1}{\pi^2}\iint_{-\infty}^{\infty} \frac{\alpha^2\eta_1^2}{\alpha^2\eta_1^2+\eta_2^2}[\mathrm{sinc}(\eta_1)\mathrm{sinc}(\eta_2)]^2 d\eta_1 d\eta_2 = \frac{1}{2\pi}\left[\alpha \ln\left(\frac{\alpha^2+1}{\alpha^2}\right) + 4\arctan\alpha - \frac{1}{\alpha}\ln\left(\alpha^2+1\right)\right] \tag{45}$$

$$S_2 = \frac{1}{\pi^2}\iint_{-\infty}^{\infty} \frac{\eta_2^2}{\alpha^2\eta_1^2+\eta_2^2}[\mathrm{sinc}(\eta_1)\mathrm{sinc}(\eta_2)]^2 d\eta_1 d\eta_2 = 1 - S_1 \tag{46}$$

$$S_3 = \frac{1}{\pi^2}\iint_{-\infty}^{\infty} \left(\frac{\alpha^2\eta_1^2}{\alpha^2\eta_1^2+\eta_2^2}\right)^2 [\mathrm{sinc}(\eta_1)\mathrm{sinc}(\eta_2)]^2 d\eta_1 d\eta_2 = \frac{1}{4\pi}\left[\alpha \ln\left(\frac{\alpha^2+1}{\alpha^2}\right) + 8\arctan\alpha - \frac{3}{\alpha}\ln\left(\alpha^2+1\right)\right] \tag{47}$$

$$S_4 = \frac{1}{\pi^2}\iint_{-\infty}^{\infty} \left(\frac{\eta_2^2}{\alpha^2\eta_1^2+\eta_2^2}\right)^2 [\mathrm{sinc}(\eta_1)\mathrm{sinc}(\eta_2)]^2 d\eta_1 d\eta_2 = \frac{1}{4\pi}\left[4\pi - 8\arctan\alpha - 3\alpha\ln\left(\frac{\alpha^2+1}{\alpha^2}\right) + \frac{1}{\alpha}\ln\left(\alpha^2+1\right)\right] \tag{48}$$

$$S_5 = (1 - S_4 - S_3)/2 \tag{49}$$

In a recent work on 2D Eshelby tensors (Zou et al., 2010), those constants are computed by using explicit expressions of complex integrals. Our paper follows a different route, via Fourier transforms (Mura, 1987; Chiu, 1977), and recovers the same results. In a special case where the inclusion is a square ($\alpha = 1$) we obtain

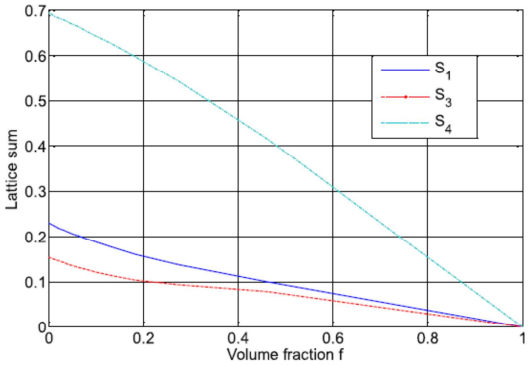

Fig. 3. Lattice sums S_1, S_3, S_4 for the rectangular inclusion arranged in CR lattice.

$$S_1 = S_2 = \frac{1}{2}, \quad S_3 = S_4 = \frac{\pi - \ln 2}{2\pi}, \quad S_5 = \frac{\ln 2}{2\pi}, \tag{50}$$

From (44) and (50), we can see a clear difference between the square shape and circular shape in the coefficients S_3, S_4, S_5. Here the discrepancies are roughly 12% in this case. Then depending on configurations, these discrepancies can have more or less impact on the overall behavior.

As an example, we carry out numerical computation of the lattice sums S_1, S_3, S_4 for inclusions with dimensions $b_1 = 100mm$, $b_2 = 25mm$ ($\alpha = 0.25$) for two cases:

- Case 1: Elliptical inclusion with PR arrangement.
- Case 1: Rectangular inclusion with CR arrangement

The vertical and horizontal distances between the inclusions are the same and varied to obtain systems with different volume fraction. The sums are taken over all wave vectors satisfying

$$|n_1| < N, \quad |n_2| < N \tag{51}$$

with $N = 1024$. Under this resolution, the lattice sums converge smoothly to the analytical values when (see Fig. 3) $f \to 0$.

According to analytical formulas (45)–(49) for the rectangular inclusions and $\alpha = 0.25$, $S_1 \to 0.2301$, $S_3 \to 0.1544$, $S_4 \to 0.6972$ when $f \to 0$. The numerical results shown in Fig. 3 and the analytical results are in very good agreement in this case. All the lattice sums tend to 0 when $f \to 1$, i.e the whole media is occupied by inclusions, which is in consistency with Eq. (25).

For elliptical inclusions, we have a simple analytical solution valid for all ranges of volume fractions. Indeed, applications of (38)–(42) with $\alpha = 0.25$ to the structure have yielded results which match perfectly the numerical solutions (see Fig. 4). The theoretical limit values are both predicted by the two solutions, i.e. $S_1 \to 0.2$, $S_3 \to 0.12$, $S_4 \to 0.72$ when $f \to 0$.

3. Determination of the overall relaxation functions

3.1. Exact inverse Laplace-Carson method

Until now, we have only examined the equivalent viscoelastic behavior of our system via the correspondence principle. Having obtained the explicit expressions for the effective moduli in terms of s variable, we need to invert the latter to find the corresponding relaxation functions of time t. Fortunately, all the expressions

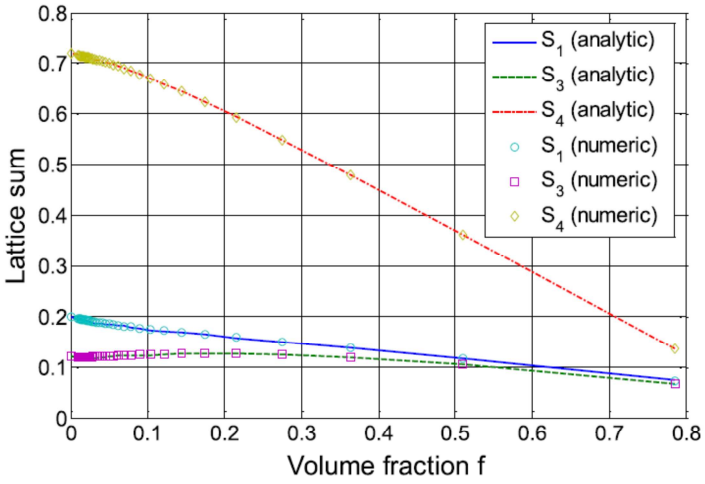

Fig. 4. Lattice sums S_1, S_3, S_4 for the elliptical inclusion arranged in PR lattice.

presented in the previous sections are rational function of s and can be inverted numerically. Given a rational function, we can always factorize the denominator and decompose the function into a sum of simpler invertible rational functions.

In the general case, it is possible to simplify significantly the expression of the effective coefficients by noticing that each combination of elastic coefficients is a rational function with a denominator containing only the denominators $d(s)$ and $D(s)$ of $k^*_0 = N(s)/D(s)$ and $\mu^*_0 = n(s)/d(s)$. Using the simplification by $d(s)$ and $D(s)$ leads to rational functions for the effective "elastic" coefficients whose polynomials in numerators and denominators are all of degree 12. However, a more careful inspection of these components of the rational function allows to factorize Δ and to reduce the degree of all polynomials to 7. Then, it is possible to compute numerically all coefficients of these polynomials and the poles of the rational function. The details of the computation are reported in the following.

The effective coefficients of Eq. (27) can be put into the form:

$$C^{e*}_{1111} = P + \frac{fC}{\Delta}$$

$$C^{e*}_{2222}\Big| = P + \frac{fA}{\Delta}$$

$$C^{e*}_{1122} = \lambda^*_0 + \frac{fB}{\Delta}$$

where $P = k^*_0 + \frac{4}{3}\mu^*_0$. The terms $A,B,C,\Delta = A.C - B^2$ can be expressed by introducing the numerators and denominators of all coefficients:

$$L = k^*_0 + \frac{1}{3}\mu^*_0,\quad M = \delta k^*_0 + \frac{4}{3}\delta\mu^*_0,\quad Q = \delta k^*_0 + \frac{1}{3}\delta\mu^*_0,\quad R = \delta k^*_0 - \frac{2}{3}\delta\mu^*_0,\quad \delta\mu^*_0$$

under the form:

$$P = \frac{n_P}{dD}, L = \frac{n_L}{dD}, M = \frac{n_M}{dD}, Q = \frac{n_Q}{dD}, R = \frac{n_R}{dD}, \delta\mu = \frac{n_{d\mu}}{d}, \delta k = \frac{n_{dk}}{D},\ \lambda^*_0 = \frac{n_\lambda}{dD},$$

where $d = d(s)$ and $D = D(s)$ are the polynomials constituting the denominators of μ^*_0 and k^*_0, while n_i are numerators of the related quantities i, are of order 1 or 2 in s. Then, the coefficients within the expressions of the effective coefficients are:

$$A = \frac{d}{4}\frac{4S_1 n_P n_{d\mu} nQ - 4S_3 n_L n_{d\mu} n_Q + n_M n_P n}{n_P n_{d\mu} n_Q n} = \frac{d}{4}\frac{n_A}{n_P n_{d\mu} n_Q n} = \gamma n_A$$

$$C = \frac{d}{4}\frac{4S_2 n_P n_{d\mu} nQ - 4S_4 n_L n_{d\mu} n_Q + n_M n_P n}{n_P n_{d\mu} n_Q n} = \frac{d}{4}\frac{n_C}{n_P n_{d\mu} n_Q n} = \gamma n_C$$

$$B = \frac{d}{4}\frac{n_R n_P n + 4S_5 n_L n_{d\mu} n_Q}{n_P n_{d\mu} n_Q n} = \frac{d}{4}\frac{n_B}{n_P n_{d\mu} n_Q n} = \gamma n_B$$

$$\Delta = \gamma^2\left(n_A n_C - n_B^2\right)$$

By mathematical manipulations, we arrive at the expressions

$$C^{e*}_{1111} = \frac{n_P\left(n_A n_C - n_B^2 + 4f n_C n_{d\mu} n_Q D\right)}{dD\left(n_A n_C - n_B^2\right)}$$

$$C^{e*}_{2222} = \frac{n_P\left(n_A n_C - n_B^2 + 4f n_A n_{d\mu} n_Q D\right)}{dD\left(n_A n_C - n_B^2\right)}$$

$$C^{e*}_{1122} = \frac{n_\lambda\left(n_A n_C - n_B^2 + 4f n_B n_{d\mu} n_Q D\right)}{dD\left(n_A n_C - n_B^2\right)}$$

A more careful examination of $n_A n_C - n_B^2$ shows that this polynomial contains the product $nDn_{d\mu}n_Q$, so that $n_A n_C - n_B^2 = 4nDn_{d\mu}n_Q\Delta_2$, with

$$\Delta_2 = d_0 + d_4(S_3+S_4) + d_{34}(S_3+S_4) + d_5 S_5 + d_{55}S_5^2 + d_{45}S_5(S_3+S_4)$$

where

$$d_0 = n_P^2 n$$
$$d_4 = \frac{1}{3}\left(3n_{dk}d + 4n_{d\mu}D\right)nn\_P$$
$$d_{34} = 4n_{d\mu}n_Q nD$$
$$d_5 = 2n_P\left(2Dn_{d\mu}n + n_{dk}dn + 2Ndn_{d\mu}\right)$$
$$d_{55} = \frac{4}{3}(5nD + 6Nd)n_{d\mu}n_Q$$
$$d_{45} = 4n_P n_Q n_{d\mu}$$

Finally, the effective coefficients are:

$$C^{e*}_{1111} = \frac{n_P(\Delta_2 + 4fn_C)}{Dd\Delta_2}$$
$$C^{e*}_{2222} = \frac{n_P(\Delta_2 + 4fn_A)}{Dd\Delta_2}$$
$$C^{e*}_{1122} = \frac{n_\lambda(\Delta_2 + 4fn_B)}{Dd\Delta_2}$$

The numerators and denominators of these rational functions are polynomials of degree 7 in the Laplace variable. The coefficients of these polynomials and the poles of each rational function $\frac{C_{ijkl}(s)}{s}$ can be easily computed by using Matlab software. All poles are simple and negative and all residues are positive in the numerical applications, which is physically satisfying.

3.2. Approximate SLS model for the overall behavior

The disadvantage of the exact method is that it is hard to obtain explicit expressions in terms of the constituent's properties and the inverse Laplace transform is analytically cumbersome for the general cases, as explained previously. Nevertheless, one can always approximate the overall behavior by the SLS model and determine correctly the parameters from the long term and short term behavior of the equivalent material. The final formulae are explicit and work for all situations, even for the anisotropic cases. As far as engineering applications are concerned, this approximation is of interest due to the simplicity and efficiency of the SLS model. All the following analytical derivations will be dedicated to this method. Different from the previous works (see e.g Nguyen and Dormieux and Kondo, 2009; Nguyen et al., 2015a), we shall present all the parameters of the SLS model in the explicit form.

Determining the parameters associated to the SLS model is tantamount to find $\mathbb{C}^e_M$, $\mathbb{C}^e_\infty$ and $\mathbb{C}^e_\nu$ from the asymptotic response of $\mathbb{C}^{e*}$ as $s\to 0$ and $s\to\infty$, or

$$\mathbb{C}^{e*}(s) = \mathbb{C}^e_M + \mathbb{C}^e_\infty + \mathscr{O}\left(\frac{1}{s}\right), \quad \mathbb{C}^{e*}(s) = \mathbb{C}^e_\infty + s\mathbb{C}^e_\nu + \mathscr{O}\left(s^2\right) \tag{52}$$

In other words, it is sufficient to expand $\mathbb{C}^{e*}$ into a power series in $1/s$ up to zeroth order and into a power series in s up to first order. To do so, we shall base on equation (21). While the asymptotic behaviors of $\mathbb{C}^*_0$ and $\mathbb{C}^*_1$ are rather straightforward

$$\mathbb{C}^*_0(s) = \mathbb{C}_M + \mathbb{C}_\infty + \mathscr{O}\left(\frac{1}{s}\right), \quad \mathbb{C}^*_0(s) = \mathbb{C}_\infty + s\mathbb{C}_\nu + \mathscr{O}\left(s^2\right), \quad \mathbb{C}^*_1(s) = \mathbb{C}_1 = cst \tag{53}$$

it is more elaborate to find the asymptotic behaviors of $[(\mathbb{C}^*_1 - \mathbb{C}^*_0)^{-1} + \langle\mathbb{P}^*\rangle_\omega]^{-1}$ from the constituting elements. We need to compute the following limits

$$\lim_{s\to\infty}\left[(\mathbb{C}^*_1 - \mathbb{C}^*_0)^{-1} + \langle\mathbb{P}^*\rangle_\omega\right]^{-1}, \ \lim_{s\to 0}\left[(\mathbb{C}^*_1 - \mathbb{C}^*_0)^{-1} + \langle\mathbb{P}^*\rangle_\omega\right]^{-1}, \ \lim_{s\to 0}\frac{d}{ds}\left[(\mathbb{C}^*_1 - \mathbb{C}^*_0)^{-1} + \langle\mathbb{P}^*\rangle_\omega\right]^{-1} \tag{54}$$

The first and second limits of (54) can be written as.

$$\lim_{s\to\infty}\left[(\mathbb{C}^*_1 - \mathbb{C}^*_0)^{-1} + \langle\mathbb{P}^*\rangle_\omega\right]^{-1} = \left[(\mathbb{C}_1 - \mathbb{C}_M - \mathbb{C}_\infty)^{-1} + \mathbb{P}_i\right]^{-1}$$
$$\lim_{s\to 0}\left[(\mathbb{C}^*_1 - \mathbb{C}^*_0)^{-1} + \langle\mathbb{P}^*\rangle_\omega\right]^{-1} = \left[(\mathbb{C}_1 - \mathbb{C}_\infty)^{-1} + \mathbb{P}_\infty\right]^{-1} \tag{55}$$

The instantaneous and long time Hill tensors $\mathbb{P}_i, \mathbb{P}_\infty$ inside the square bracket of (55) can be calculated based on (22), for example

$$\mathbb{P}_i = \lim_{s\to\infty}\langle\mathbb{P}^*\rangle_\omega = \frac{1}{2(\mu_\infty + \mu_M)}\mathbb{W} - \frac{(k_\infty + k_M) + \frac{1}{3}(\mu_\infty + \mu_M)}{(\mu_\infty + \mu_M)\left(k_\infty + k_M + \frac{4}{3}(\mu_\infty + \mu_M)\right)}\mathbb{U},$$
$$\mathbb{P}_\infty = \lim_{s\to 0}\langle\mathbb{P}^*\rangle_\omega = \frac{1}{2\mu_\infty}\mathbb{W} - \frac{k_\infty + \frac{1}{3}\mu_\infty}{\mu_\infty\left(k_\infty + \frac{4}{3}\mu_\infty\right)}\mathbb{U}, \tag{56}$$

Finally, the last limit of (54) will now be treated. From the following properties

$$\frac{d(\mathbb{A}^{-1})}{ds} = -\mathbb{A}^{-1} : \frac{d(\mathbb{A})}{ds} : \mathbb{A}^{-1} \quad \forall\,\mathbb{A}, \tag{57}$$

we can write

$$\lim_{s\to 0}\frac{d}{ds}\left[(\mathbb{C}^*_1 - \mathbb{C}^*_0)^{-1} + \langle\mathbb{P}^*\rangle_\omega\right]^{-1} = -\left[(\mathbb{C}_1 - \mathbb{C}_\infty)^{-1} + \mathbb{P}_\infty\right]^{-1} : : \left[(\mathbb{C}_1 - \mathbb{C}_\infty)^{-1} : \mathbb{C}_\nu : (\mathbb{C}_1 - \mathbb{C}_\infty)^{-1} + \mathbb{P}_\nu\right] : \left[(\mathbb{C}_1 - \mathbb{C}_\infty)^{-1} + \mathbb{P}_\infty\right]^{-1} \tag{58}$$

with the Hill viscous tensor $\mathbb{P}_v$ being computed by

$$\begin{aligned}\mathbb{P}_v &= \lim_{s\to 0}\frac{d}{ds}\langle \mathbb{P}^*\rangle_\omega \\ &= \lim_{s\to 0}\frac{d}{ds}\left(\frac{1}{2\mu_0^*}\right)\mathbb{W} - \lim_{s\to 0}\frac{d}{ds}\left(\frac{k_0^*+\frac{1}{3}\mu_0^*}{\mu_0^*\left(k_0^*+\frac{4}{3}\mu_0^*\right)}\right)\mathbb{U}\end{aligned} \tag{59}$$

by some mathematical manipulations, we arrive at the result

$$\begin{aligned}\mathbb{P}_v = -\frac{\mu_v}{2\mu_\infty^2}\mathbb{W} - \Bigg[&\frac{\left(k_v+\frac{1}{3}\mu_v\right)}{\mu_\infty\left(k_\infty+\frac{4}{3}\mu_\infty\right)} - \frac{\left(k_\infty+\frac{1}{3}\mu_\infty\right)\mu_v}{\mu_\infty^2\left(k_\infty+\frac{4}{3}\mu_\infty\right)} \\ &- \frac{\left(k_\infty+\frac{1}{3}\mu_\infty\right)\left(k_v+\frac{4}{3}\mu_v\right)}{\mu_\infty\left(k_\infty+\frac{4}{3}\mu_\infty\right)^2}\Bigg]\mathbb{U}\end{aligned} \tag{60}$$

At this step, all the tensors are explicit, for example

$$\begin{aligned}\mathbb{C}_\infty^e &= \mathbb{C}_\infty + f\left[(\mathbb{C}_1-\mathbb{C}_\infty)^{-1}+\mathbb{P}_\infty\right]^{-1}, \\ \mathbb{C}_v^e &= \mathbb{C}_v - f\left[(\mathbb{C}_1-\mathbb{C}_\infty)^{-1}+\mathbb{P}_\infty\right]^{-1} : \left[(\mathbb{C}_1-\mathbb{C}_\infty)^{-1} : \mathbb{C}_v : (\mathbb{C}_1-\mathbb{C}_\infty)^{-1}+\mathbb{P}_v\right] : \left[(\mathbb{C}_1-\mathbb{C}_\infty)^{-1}+\mathbb{P}_\infty\right]^{-1}, \\ \mathbb{C}_M^e &= \mathbb{C}_M + f\left\{\left[(\mathbb{C}_1-\mathbb{C}_M-\mathbb{C}_\infty)^{-1}+\mathbb{P}_i\right]^{-1} - \left[(\mathbb{C}_1-\mathbb{C}_\infty)^{-1}+\mathbb{P}_\infty\right]^{-1}\right\}\end{aligned} \tag{61}$$

and can be applied in the examples.

4. Numerical applications

4.1. Geometry and material data of the periodic structure

To illustrate the validness of the analytical solutions derived in previous sections, we consider a particular case where the matrix and the inclusions are respectively made of mortar and brick materials. The viscoelastic properties of the constituent materials are given in Table 1.

The shapes of the inclusions can be rectangular, square, elliptical or circular. The dimensions $b_1,\ b_2$ are given in consistency with the theory presented previously.

- Rectangular (RE) or elliptical (EL) shape: $b_1 = 100mm,\ b_2 = 25mm$

The corresponding sizes of the unit cell $a_1,\ a_2$ depend on the distance between the inclusions $2e_1, 2e_2$ along. x_1, x_2

- PR lattice: $a_1 = 2(b_1+e_1),\ a_2 = 2(b_2+e_2)$,
- CR lattice: $a_1 = 2(b_1+e_1),\ a_2 = 4(b_2+e_2)$,

In this paper, we set $e_1 = e_2 = e$, and adjust e in order to obtain systems with different inclusion volume fractions f. As a remark, when the inclusions are rectangular, our structures can be used to model wall masonry. The PR and CR lattices correspond respectively to the stack bond and running bond systems. However, here we have solved the problem in a much more general context.

Table 1
Viscoelastic properties of matrix and inclusion used for the simulations (Nguyen et al., 2015a).

Parameters	Values	Units
k_M	2.404	*GPa*
μ_M	1.655	*GPa*
k_v	23.639	*GPa.h*
μ_v	21.375	*GPa.h*
k_∞	1.257	*GPa*
μ_∞	0.866	*GPa*
k_1	6.111	*GPa*
μ_1	4.583	*GPa*

4.2. Assessment of the accuracy of the analytical solution in LC space

As noted, our solution in LC space is based on the estimation of the eigenstrain in the inclusion. This approximation allows us to obtain a simple analytical solution which separates the influences of stiffness from geometry and facilitates the derivation of the overall model. The accuracy of this approximation and its impact on the overall properties depends on many factors: the inclusion shape, the inclusion volume fraction, the arrangement and the rigidity contrast. Numerical experiences on spherical inclusion have shown that with moderate rigidity contrast (less than 10) and volume fraction (less than 0.5), this approximation works very well. In the present work, the brick is 2–5 times more rigid than the mortar, suggesting that our estimation can yield good results in this working range. To judge the quality in more details, we compare our estimation with the Finite Element Method.

We consider two cases: rectangular inclusion with CR lattice and elliptical inclusion with PR lattice. The long term properties of the mortar $k_\infty,\ \mu_\infty$ are used, which corresponds to the highest possible contrast ratio between equivalent elastic properties in LC space for different values of s. The symmetry and anti-symmetry conditions are combined with the periodicity boundary conditions to reduce the computation domain by 1/4. Fig. 5 shows that the strain and stress inside the rectangular inclusion are not uniform. Furthermore, strong stress concentration and strain localization are observed at the corner of the brick. Theoretically, stresses and strains are singular as predicted by singularity analyses on bimaterial wedges (Vu et al., 2015). Careful mesh refinement at this corner allowed us to take into account those effects on the overall properties. For elliptical inclusions, Fig. 6 shows that the stress and strain distributions are not uniform but the variation is slight. We note that at that high volume fraction, the strong interaction at close distance between the inclusions is responsible for the deviation from the Eshelby results.

Despite those observations on the non uniformity of the stress and strain, the agreement between the FEM and the analytical results is very good for the whole volume fraction (see Table 2). The maximal discrepancies are of order 1%, which can be considered as negligible. This can be explained as being due to the moderate rigidity contrast. In this case, our estimation can capture accurately the interaction between inclusions. This agreement implies that the

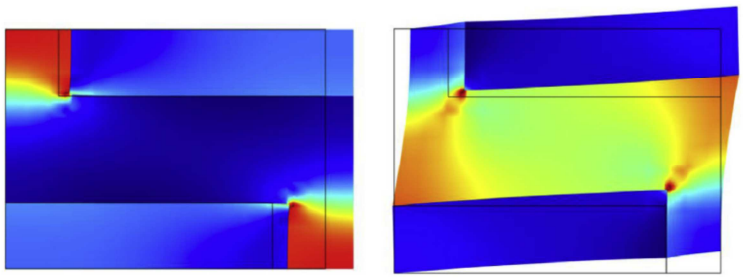

Fig. 5. Distribution of strain energy obtained by FEM method for rectangular inclusion and CR lattice. The left figure corresponds to the direct strain loading $E_{11} = 1$ (the remaining strain components $E_{22} = E_{12} = 0$) and the right figure the shear strain loading $E_{12} = 1$ (the remaining strain components $E_{22} = E_{11} = 0$).

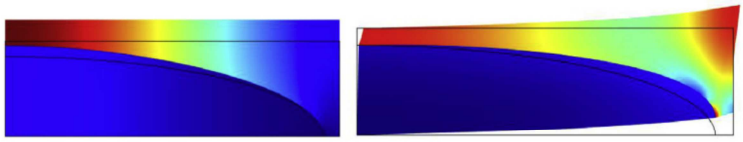

Fig. 6. Distribution of strain energy obtained by FEM method for elliptical inclusion and PR lattice. The left figure corresponds to the direct strain loading $E_{22} = 1$ (the remaining strain components $E_{11} = E_{12} = 0$) and the right figure the shear strain loading $E_{12} = 1$ (the remaining strain components $E_{11} = E_{22} = 0$).

Table 2
Comparison between FEM solution and approximate analytical solution.

f	Stiffness [GPa] by FEM solution				Stiffness [GPa] by analytical solution			
	C_{1111}	C_{2222}	C_{1122}	C_{1212}	C_{1111}	C_{2222}	C_{1122}	C_{1212}
Rectangular inclusion – CR lattice								
1	12.22	12.22	3.056	4.58	12.22	12.22	3.056	4.58
0.794	9.010	7.050	1.710	4.973	8.924	7.008	1.714	4.917
0.649	7.280	5.360	1.330	3.785	7.156	5.306	1.345	3.734
0.463	5.420	4.030	1.070	2.890	5.317	3.989	1.082	2.854
0.275	3.920	3.180	0.900	2.310	3.869	3.164	0.904	2.295
0.132	3.050	2.730	0.780	1.980	3.025	2.730	0.782	1.976
0	2.412	2.412	0.680	1.732	2.412	2.412	0.680	1.732
Elliptical inclusion – PR lattice								
0.623	6.71	5.35	1.27	3.61	6.5411	5.2196	1.2624	3.5658
0.510	5.64	4.39	1.09	3.02	5.5832	4.3458	1.0879	3.0067
0.364	4.50	3.56	0.93	2.5	4.496	3.5508	0.9353	2.4993
0.216	3.54	2.98	0.82	2.13	3.5405	2.9827	0.8241	2.1317
0.104	2.91	2.65	0.75	1.91	2.9094	2.6564	0.751	1.9119
0.000	2.412	2.412	0.680	1.732	2.412	2.412	0.680	1.732

simple analytical solution can allow to derive the coefficients entering the overall constitutive equations with a good precision.

4.3. Parametric study of the approximate model

Figs. 7–9 show the effective viscoelastic properties of the mixture as functions of the volume fraction of brick. There are three effective viscoelastic tensors due to the chosen Zener's viscoelastic rheological model for the overall behavior of the material. Each tensor has four independent viscoelastic parameters due to the 2D orthotropic anisotropy of the mixture that is a result of the rectangular shape of the brick. Figs. 7 and 8 show the long-term effective elastic stiffnesses and the one of the Maxwell's series, respectively.

Fig. 9 presents the effective viscous parameters entering the Maxwell's series. The components C_{1111} and C_{2222} coincide when the volume fraction of inclusions f tends to 0 or 1 due to the isotropy of the matrix and inclusions. However they are very different when the concentration of inclusions reaches about 60–80%. Similar trends are obtained for the terms C_{1212} and C_{1122}. It is interesting to observe that all the elastic stiffnesses and the viscosities of the Maxwell's series tend to zero when the volume fraction of brick tends to 1, as expected since an elastic behavior is assumed for brick inclusion. More precisely, the viscous behavior of masonry originated by that of the mortar matrix vanishes when the volume fraction of mortar tends to zero. Similar observations for the case of elliptic inclusions are shown on Figs. 10–12. A comparison between the two kinds of inclusions is also shown on Fig. 13. The close results obtained for rectangular and elliptic inclusions may be due to the same values of $b_1 = 100mm$, $b_2 = 25mm$ used for defining the geometry of the cell.

4.4. Comparison between the relaxation behaviors obtained via the approximate model and the exact inversion

As explained in subsection 3.1, the inversion of the expression of the effective coefficients in the Laplace space can be computed by using the expressions for the poles and residues of the involved rational fractions. Then, the inversion can be performed explicitly and compared with the approximate model. After comparison on numerical results in a few cases, we have found that the difference between the two approaches is less than 1%.

As an example, we consider the case of rectangular inclusion and CR lattice and the component C^{e*}_{2222}. The geometric parameters of the system are $b_1 = 100mm, b_2 = 25mm$ and $a_1 = 240mm, a_2 = 180mm$. After simplification and inversion, the relaxation component $C^{e}_{2222(ex)}$ is given by the expression

$$\begin{aligned} C^{e}_{2222(ex)}(t) = {} & 3.988 + 0.0021e^{-0.028t} + 0.0009e^{-0.0399t} \\ & + 3.5597e^{-0.0617t} + 0.2490e^{-0.0774t} \\ & + 0.0165e^{-0.0889t} + 0.979e^{-0.0946t} \\ & + 0.0194e^{-0.1017t} \end{aligned} \tag{62}$$

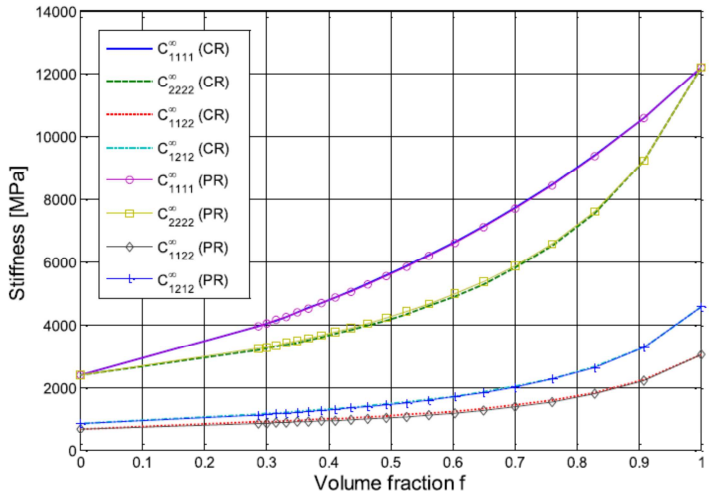

Fig. 7. Influence of lattice type on the coefficients of the long-term stiffness tensor $\mathbb{C}^e_\infty$ as functions of the volume fraction of the rectangular inclusions.

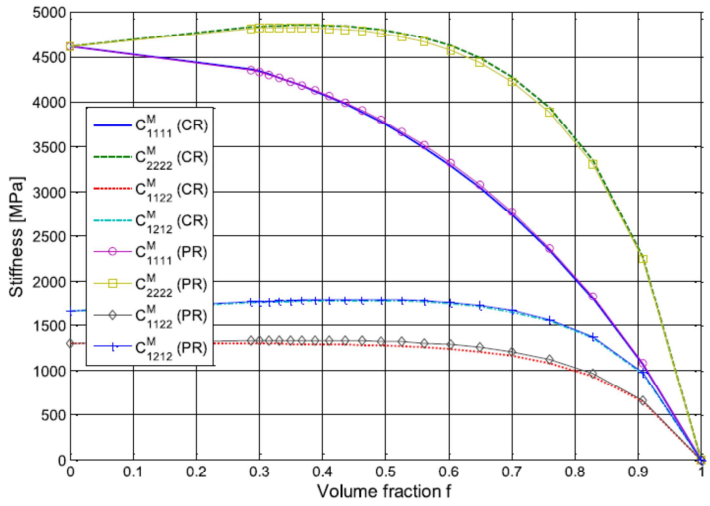

Fig. 8. Influence of lattice type on the coefficients of the stiffness tensor $\mathbb{C}^e_M$ as functions of the volume fraction of the rectangular inclusions.

The relaxation function of the approximate SLS model is the following

$$C^e_{2222(SLS)}(t) = 3.988 + 4.23e^{-0.0695t} + 0.5958e^{-0.0549t} \tag{63}$$

Using **(62)** and **(63)**, we can plot the relaxation functions in Fig. 14. We find that the two curves are extremely close. Both curves capture well the short and long time modulus and the required time for full relaxation, that is around 80–100 h.

Next we study the differences in detail. Fig. 15 shows the relative difference $r = \frac{C_{(SLS)} - C_{(ex)}}{C_{(ex)}}$ in the case of rectangular inclusions for the coefficient C_{2222}. The figure shows that the relative difference is always inferior to 4.10^{-3}, proving that the SLS model represents well the overall behavior.

Suquet (2012) studied composites constituted of matrix and inclusion, both being characterized by a viscoelastic behavior of Maxwell type. In this paper, numerical tests based on a linear loading followed by a harmonic loading have exhibited significant differences between a Maxwell approximate model and the real overall behavior. By comparison, we have also carried out a test involving a loading similar to the one used in Suquet (2012) where the strain history along direction 2 is the following function of time

$$\varepsilon_{22} = 0.01t \ \text{ for } t<20, \quad \varepsilon_{22} = 0.2 + 0.01\sin(t-20) \text{ for } t>20 \tag{64}$$

The remaining strain components are maintained zero throughout the test. Fig. 16 shows that the responses $\sigma_{22}(t)$ of the two models are very close. This again confirms the accuracy of the present approximation, as already observed in the literature when

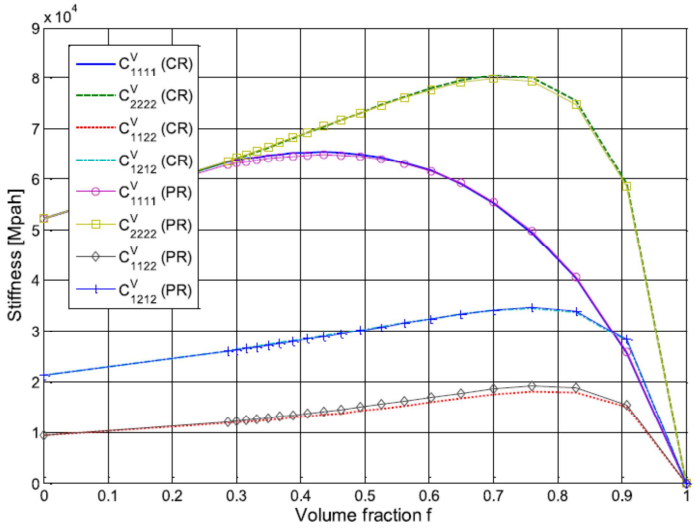

Fig. 9. Influence of lattice type on the coefficients of the viscosity tensor $\mathbb{C}_f^e$ as functions of the volume fraction of the rectangular inclusions.

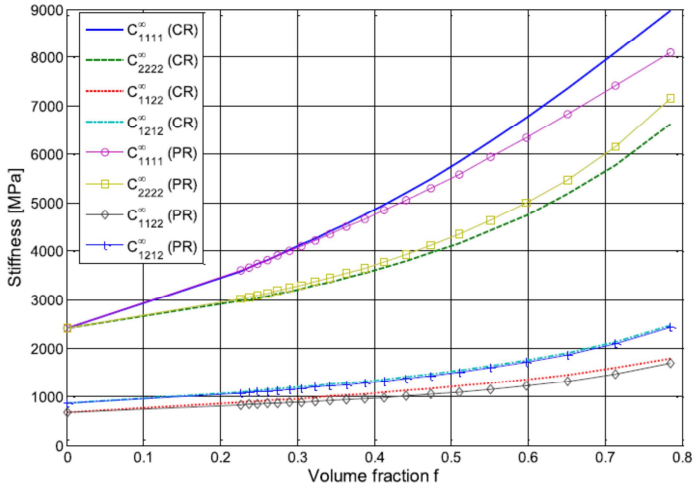

Fig. 10. Influence of lattice type on the coefficients of the long-term stiffness tensor $\mathbb{C}_\infty^e$ as functions of the volume fraction of the elliptical inclusions.

the inclusions are elastic (including the cases of void and rigid inclusions), i.e. when only one of the constituents displays a relaxation time. In comparison, the computations reported in Suquet (2012) involve two fully viscoelastic materials, and therefore two relaxation times, which can explain qualitatively the difference between our results and these earlier results.

We have also performed calculations using different geometries (elliptical inclusion or PR lattice) and find very small differences. These observations are very interesting since the approximate model is much simpler than the full inversion method. While the strategy of the direct inversion method seems to be trivial, the symbolic calculation is very cumbersome. In our experience, this calculation is also difficult and can be erroneous without some careful inspection and elimination of common roots between the numerators and denominators. From those perspectives, the simplicity and the ability to capture the real relaxation behavior are the main advantages of the approximate model. That will be the main conclusion of this paper.

5. Conclusions and perspectives

In this paper, analytical and numerical solutions for the overall viscoelastic properties of 2D periodic structures are presented. Under the plane strain hypothesis, the effective properties are

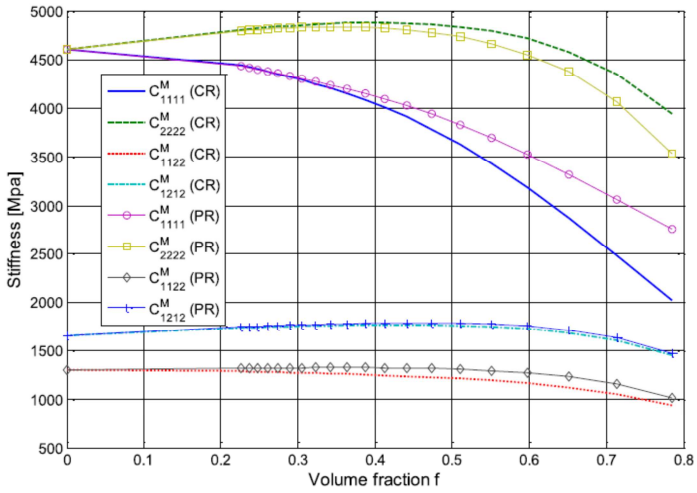

Fig. 11. Influence of lattice type on the coefficients of the stiffness tensor $\mathbb{C}^e_M$ as functions of the volume fraction of the elliptical inclusions.

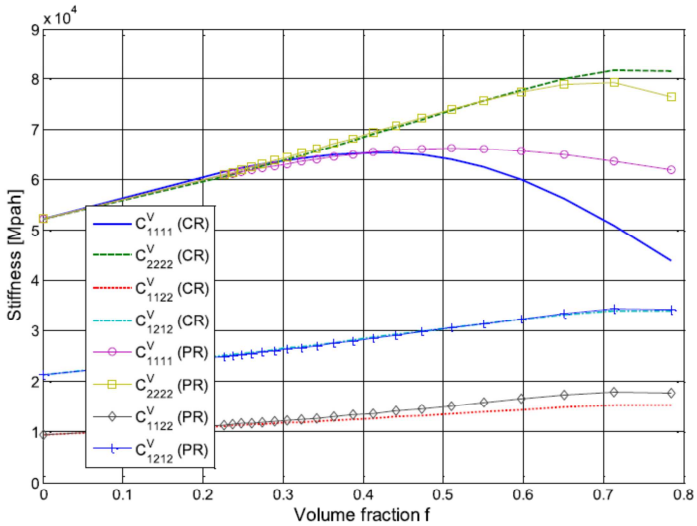

Fig. 12. Influence of lattice type on the coefficients of the stiffness tensor $\mathbb{C}^e_v$ as functions of the volume fraction of the elliptical inclusions.

obtained explicitly in LC space first. Here, we have used the solution technique based on integral equation approach and Fourier transform, which has proved to yield a good estimation of the effective properties. Due to the inclusion shapes (ellipse or rectangle) and the distribution (PR or CR lattices), the equivalent material is viscoelastic and anisotropic in the considered plane. After deriving the overall moduli in LC space, two inversion methods are proposed to obtain the results in time space, that is the relaxation behavior. The first one is to calculate directly the inverse of the LC transform through the decomposition into simple rational fractions, that leads to exact solutions. The second one is to approximate the equivalent media with a Standard Linear Solid model and to determine accurately the parameters based on studies of asymptotic behavior at short and long time scale.

Finally, applications to masonry structures are presented. The validation of the approximate homogenization scheme has been performed successfully by comparison with the results of a FEM modelling. At the same time, the results have shown a good agreement between complete LC inversion and the approximate one. A noticeable influence of both inclusion shapes and distribution has been obtained. It is important to mention that our results were obtained in the case of a moderate contrast between inclusion and matrix and cannot be generalized for very large contrasts.

Based on the estimation in LC space and the approximation

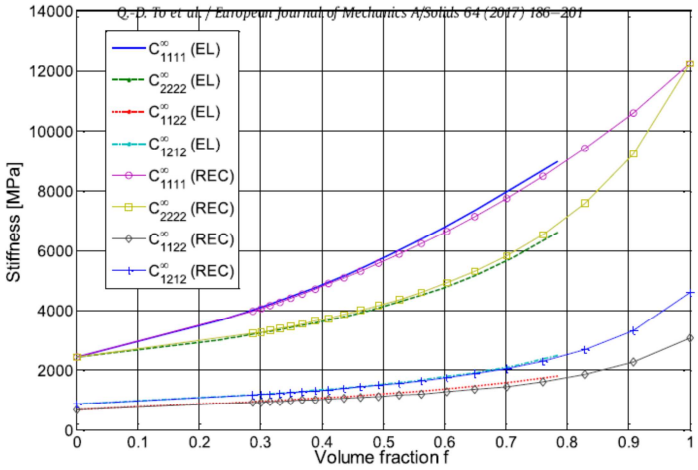

Fig. 13. Influence of inclusion shapes (rectangle or ellipse) on the long-term stiffness tensor $\mathbb{C}^{e}_{\infty}$ as functions of the volume fraction of the inclusions. The lattice type is centered rectangular.

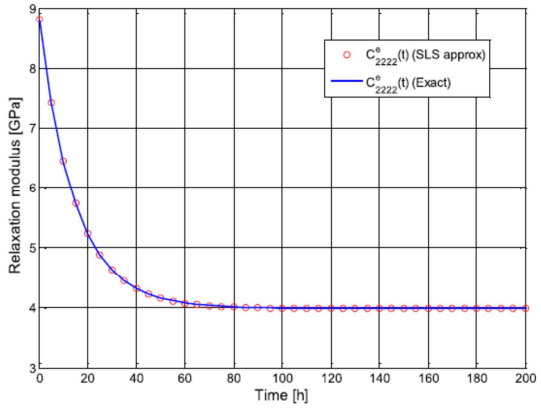

Fig. 14. Exact relaxation function $C_{2222(ex)}(t)$ and the approximate relaxation function $C_{2222(SLS)}(t)$ for rectangular inclusions, CR lattice.

model via the asymptotic study of LC variable s, the present approach can be extended to deal with a general hereditary integral form. Obviously, the exact inversion of Laplace transform can become more and more cumbersome when the number of relaxation times increases, but the derivation of the approximate SLS can be easily derived as shown in section 3.

In addition, we must acknowledge that under extreme situations where a strong rigidity contrast is combined with high concentration of inclusions and multiple relaxation times, the estimations in the current form may not be sufficient. However, it can be shown in the case of elastic materials that the model described in section 2 corresponds to the first order of an expansion in correlation functions characterizing the distribution of inclusions. Consequently, improvements can be done by using higher order correlations of material distribution (Nguyen et al., 2016; To et al., 2016b) and higher order expansion of the exact relaxation function (Nguyen, 2014; Nguyen et al., 2015b). Those aspects will be investigated in a future work.

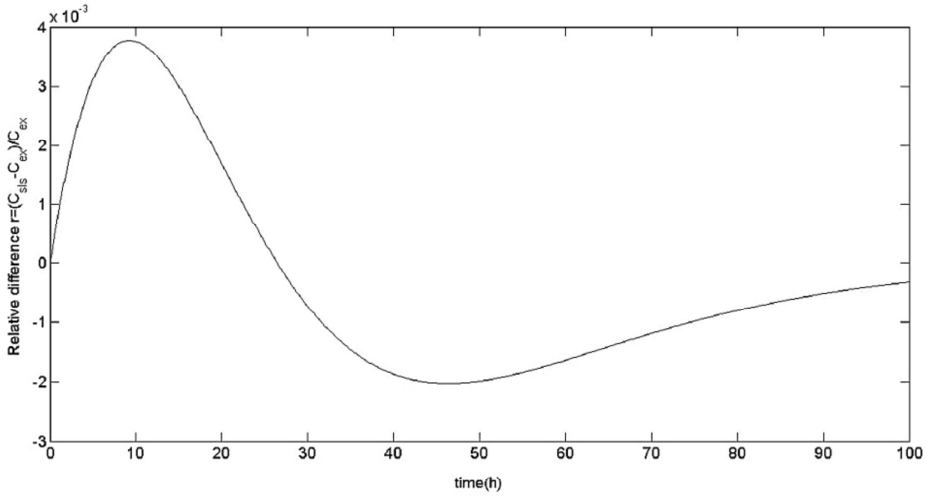

Fig. 15. Relative difference between the exact relaxation function $C_{2222(ex)}(t)$ and the approximate relaxation function $C_{2222(SLS)}(t)$ for rectangular inclusions and CR lattice.

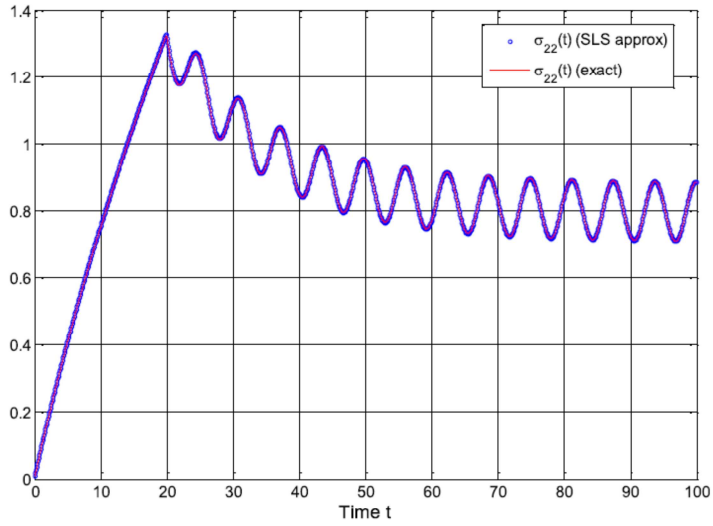

Fig. 16. Response to linear - harmonic loading for rectangular inclusions and CR lattice.

A last issue concerns the thermomechanical coupling, because most polymers are viscoelastic and also sensitive to temperature. The results presented previously can be used without further work in the case of weak coupling characterized by a moderate temperature dependence of viscosities and elasticity tensors (see e.g Francfort and Suquet, 1986). Concerning the full thermoviscoelastic coupling, the method used in this paper is obviously restricted to a spatial linear behavior in LC space. In this context, the extension of the methodology presented here to thermoviscoelasticity is feasible and would be of interest in particular for applications to composites with a polymer matrix.

References

Benveniste, Y., Milton, G., 2003. New exact results for the effective electric, elastic, piezoelectric and other properties of composite ellipsoid assemblages. J. Mech. Phys. Solids 51, 1773–1813.

Christensen, R.M., 1969. Viscoelastic properties of heterogeneous media. J. Mech. Phys. Solids 17 (1), 23–41.

Christensen, R., Lo, K., 1979. Solutions for effective shear properties in three phase sphere and cylinder models. J. Mech. Phys. Solids 27, 315–330.

Chiu, Y.P., 1977. On the stress field due to initial strains in a cuboid surrounded by an infinite elastic space. J. Appl. Mech. 44, 587–590.

Dormieux, L., Kondo, D., 2009. Stress-based estimates and bounds of effective elastic properties: the case of cracked media with unilateral effects. Comput. Mater. Sci. 46 (1), 173–179.

Dormieux, L., Kondo, D., Ulm, F.J., 2006. Microporomechanics. John Wiley & Sons, Chichester.

Eshelby, J., 1957. The determination of the elastic field of an ellipsoidal inclusion, and related problems. Proc. R. Soc. Lond. A 241, 376–396.

Eyre, D.J., Milton, G.W., 1999. A fast numerical scheme for computing the response of composites using grid refinement. Eur. Phys. J. Appl. Phys. 6, 41–47.

Francfort, G.A., Suquet, P., 1986. Homogenization and mechanical dissipation in thermoviscoelasticity. Archive Ration. Mech. Anal. 96, 265–293.

Hashin, Z., Shtrikman, S., 1963. A variational approach to the theory of the elastic behaviour of multiphase materials. J. Mech. Phys. Solids 11, 127–140.

Hashin, Z., 1965. Viscoelastic behavior of heterogeneous media. J. Appl. Mech. Trans. ASME 32, 630–636.

Hashin, Z., 1970. Complex moduli of viscoelastic composites - I. General theory and application to particulate composites. Int. J. Solids Struct. 6, 539–552.

Hill, R., 1965. A self-consistent mechanics of composite materials. J. Mech. Phys. Solids 13, 213–222.

Hoang, D.H., Bonnet, G., 2013. Effective properties of viscoelastic heterogeneous periodic media: an approximate solution accounting for the distribution of heterogeneities. Mech. Mater. 56, 71–83.

Kachanov, M., 1992. Effective elastic properties of cracked solids: critical review of some basic concepts. Appl. Mech. Rev. 45 (8), 304–335.

Lahellec, N., Suquet, P., 2007. Effective behavior of linear viscoelastic composites: a time-integration approach. Int. J. Solids Struct. 44 (2), 507–529.

Le, Q.V., Meftah, F., He, Q.C., Le Pape, Y., 2007. Creep and relaxation functions of a heterogeneous viscoelastic porous medium using the Mori-Tanaka homogenization scheme and a discrete microscopic retardation spectrum. Mech. Time-Dependent Mater. 11 (3–4), 309–331.

Lévesque, M., Gilchrist, M.D., Bouleau, N., Derrien, K., Baptiste, D., 2007. Numerical inversion of the Laplace–Carson transform applied to homogenization of randomly reinforced linear viscoelastic media. Comput. Mech. 40 (4), 771–789.

Michel, J., Moulinec, H., Suquet, P., 1999. Effective properties of composite materials with periodic microstructure: a computational approach. Comput. Methods Appl. Mech. Eng. 172, 109–143.

Monchiet, V., Bonnet, G., 2012. A polarization based FFT iterative scheme for computing the effective properties of elastic composites with arbitrary contrast. Int. J. Numer. Meth. Eng. 89, 1419–1436.

Mori, T., Tanaka, K., 1973. Average stress in matrix and average elastic energy of materials with mistting inclusions. Acta Metall. Mater. 21, 571–574.

Mura, T., 1987. Micromechanics of Defects in Solids. Kluwer Academic Publisher, New York.

Nemat-Nasser, S., Iwakuma, T., Hejazi, M., 1982. On composites with periodic structure. Mech. Mater. 1, 239–267.

Nemat-Nasser, S., Hori, M., 1993. Micromechanics : Overall Properties of Heterogeneous Materials. Elsevier, New York.

Nguyen, M.T., Monchiet, V., Bonnet, G., To, Q.D., 2016. Conductivity estimates of spherical-particle suspensions based on triplet structure factors. Phys. Rev. E 93, 022105.

Nguyen, S.T., Dormieux, L., Le Pape, Y., Sanahuja, J., 2011. A Burger model for the effective behavior of a microcracked viscoelastic solid. Int. J. Damage Mech. 20 (8), 1116–1129.

Nguyen, S.T., 2014. Generalized Kelvin model for micro-cracked viscoelastic materials. Eng. Fract. Mech. 127, 226–234.

Nguyen, T.N., Nguyen, S.T., Vu, M.H., Vu, M.N., 2015a. Effective viscoelastic properties of micro-cracked heterogeneous materials. Int. J. Damage Mech. 25 (4), 557–573.

Nguyen, S.T., Vu, M.H., Vu, M.N., Nguyen, T.N., 2015b. Generalized Maxwell model for micro-cracked viscoelastic materials. Int. J. Damage Mech. (in press).

Schapery, R.A., 1967. Stress analysis of viscoelastic composite materials. J. Compos. Mater. 1 (3), 228–267.

Suquet, P., 2012. Four exact relations for the effective relaxation function of linear viscoelastic composites. Compte Rendu Mécanique 4 (3), 387–399.

To, Q.D., Bonnet, G., To, V.T., 2013. Closed-form solutions for the effective conductivity of two-phase periodic composites with spherical inclusions. Proc. Roy. Soc. A 469 paper n°20120339.

To, Q.D., Bonnet, G., Hoang, D.H., 2016a. Explicit effective elasticity tensors of two-phase periodic composites with spherical or ellipsoidal inclusions. Int. J. Solids Struct. 94, 110–111.

To, Q.D., Nguyen, M.T., Bonnet, G., Monchiet, V., To, V.T., 2016b. Overall Elastic Properties of Composites from Optimal Neumann Series and n-th Order Structure Factors (submitted).

Vu, M.N., Geniaut, S., Massin, P., Marigo, J.J., 2015. Numerical investigation on corner singularities in cracked plates using the G-theta method with an adapted θ field. Theor. Appl. Fract. Mech. 77, 59–68.

Wang, Y.M., Weng, G.J., 1992. The influence of inclusion shape on the overall viscoelastic behavior of composites. J. Appl. Mech. 59 (3), 510–518.

Zou, W., He, Q.C., Huang, M., Zheng, Q.S., 2010. Eshelby's problem of non-elliptical inclusions. J. Mech. Phys. Solids 58 (3), 346–372.